Entropy generation during peristaltically flowing nanofluid in an axisymmetric channel with flexible walls

M N Abrar, M Sagheer and S Hussain

Department of Mathematics, Capital University of Science and Technology, Zone V Express way, Islamabad 44000, Pakistan

E-mail: muhammad.nasir@cust.edu.pk and nasirabrar10@gmail.com

Abstract

This study investigates the entropy generation analysis of creeping viscous nanofluid flow influenced by metachronical waves in a horizontal ciliated tube containing porous medium along inclined magnetic field. Water based silicon dioxide (SiO_2) nanofluid is studied with an effects of various shaped nanoparticles. Hamilton–Crosser model is considered for the effective thermal conductivity of the nanofluids. One of the way to increase heat transfer is to employ porous medium with nanofluid. Moreover, impact of Joule heating, viscous dissipation and internal heat source is also taken into the consideration in the heat transfer mechanism. Mathematical formulation has been completed, which results into a set of ordinary differential equations. Exact solutions in the closed form have been computed for the momentum, pressure gradient and energy profiles respectively. The impact of Darcy phenomena with emerging flow parameters are graphed for pure and diluted water on velocity profile. Three dimensional bar graphs are also designed to show the variation of local Nusselt number in order to measure the rate of heat transfer. It is seen that an increasing magnitude of Hartmann number reduces the flow velocity. Further, maximum entropy is seen at the bottom of the axisymmetric channel and least near the ciliated walls.

Keywords: entropy analysis, inclination angle, ciliated walls, porous medium, bricks and cylinders nanoparticles

(Some figures may appear in colour only in the online journal)

Nomenclature

nf	nanofluid
β	Wave number
s	Solid nanoparticles
ξ	Angle of inclination
θ	Dimensionless temperature
Ω	Heat source coefficient
K	Permeability parameter
ρ_{nf}	Effective density of the nanofluid
ρC_p	Heat capacitance
ϕ	Solid volume fraction of nanofluid
λ	Wavelength of the metachronal wave
Λ	Dimensionless temperature difference
k_{bf}	Thermal conductivity of the base fluid
ϵ	Wave amplitude
μ_{nf}	Effective dynamic viscosity of the nanofluid
α	Measure of the eccentricity of the elliptical motion
bf	Base fluid
B_0	Magnetic field
Br	Brinkman number
E_G	Entropy number

Ha	Hartmann number
$\hbar$	Height of the tube
J_h	Joule heating
w	Dimensionless velocity
e	Mean radius of the tube
α_nf	Effective thermal diffusivity
k_nf	Effective thermal conductivity
$\overline{T}$	Local temperature of the fluid
$\overline{Z_0}$	Reference position of the particle
Q_0	Internal heat source
c	Wave speed of the metachronal wave

1. Introduction

In the last era as energy crises are emerging rapidly, there has been a massive need for new procedures which can increase thermal efficiency of working fluid and thus reduces overall energy crises. In order to overcome the energy crises, wavy surfaces, micro channels, vibration phenomenon, etc are developed by researchers and engineers to reinforce the heat transfer rate. In 1995, Choi [1] intially introduced the term nanofluid which describe that the heat transfer rate can be enhanced by improving the thermal conductivity of base fluids. As base fluids, like pure water, lubricants etc, possess finite heat transfer strength because of their low thermal abilities. On contrary, nanoparticles holds dramatically higher thermal strenght as compared to base fluids. Moreover, nanofluid offer their potential application in chemical, biological and earth engineering, for example, pharmaceutical transport [2], magnetic resonance technology [3], safe drinking water [4]. It is a very common practice in circumpolar world (where the temperature is alomost less then $40°$ throughout the years) to use nanoparticles with water as a heat transfer fluid [5]. To be specific to our case: silicon dioxide has seen exceptional application in fuel cells [6], solar collector [7], etc. Based on the these useful application of nanoparticles. After Choi, on the subject of nanofluid with different geometries has been discussed by a very big number of researchers e.g. Abrar and Awais [8], Estellé *et al* [9], Abrar *et al* [10], Turkyilmazoglu and Pop [11], Hussain *et al* [12], Garoosi *et al* [13], Nield and Kuznetsov [14], Sheikholeslami *et al* [15], Akbar and Butt [16], Abrar *et al* [17], Avramenko *et al* [18], Yadav [19], Rana *et al* [20], Yadav and Lee [21], Ali *et al* [22], Abrar *et al* [23], Hamzah *et al* [24], Sheremet *et al* [25], Sheremet *et al* [26], Alam *et al* [27], Yadav [28, 29], Sheikholeslami *et al* [30].

The efficiency of any engineering machine containing thermofluid strongly relies upon the structure and the running temperature of the functioning fluid. Since the heat transfer is an irreversible mechanism, therefore, for the outstanding performance of system, it is necessary to inspect the entropy of system. The second law of thermodynamics is imposed to investigate the irreversibilities in a system in terms of entropy.

Entropy defines the system's thermal energy per unit temperature that is not available for performing some useful work. The entropy of the system can be computed by using the second law of thermodynamics. The latest studies have demonstrated that the second law investigation approach is an effective and productive strategy for reducing the entropy of the system. The entropy formation is connected with a large number of energy relevant procedures such as geothermal power systems and solar power systems. Firstly, Bejan [31] describe the knowledge of entropy in heat transfer and fluid flow systems. Makinde *et al* [32], Aksoy [33], Rashidi *et al* [34], Hussain *et al* [35], Kamran *et al* [36], Abrar *et al* [37], Adesanya and Fakoya [38], Nadezhda *et al* [39], Marina *et al* [40], have recently contributed in this useful area of entropy analysis by considering different physical and engineering scenarios.

In any engineering procedure, there are many ways to increase the rate of heat transfer, one of them is using porous media in heat transfer appliances. Porous media is basically a material which consists of solid matrix with an interconnected void spaces, for example rocks and open cell aluminum foams [41]. The process of using porous material has been the core subject of multiple studies and has taken a rational appreciation. This appreciation is because of the fact that this type of structure is highly acceptable in many engineering applications, such as thermal insulation, oil flow, ground water, power stations, etc. Porous medium is specially applied in such kinds of engineering devices, where the cooling or heating is mandatory, like cooling turbine blades, cooling electronic equipment, etc. The mixing of the low and high energy fluids which happens in above applications significantly influence the working of these devices [42, 43].

The main objective of this study is to examine the entropy generation due to heat transfer, viscous dissipation and magnetic field in an axisymmetric channel with flexible walls having porous medium. The principal interest of considering porous medium is two in numbers. Firstly, its dissipation area is larger than the traditional fins that boost the rate of heat transfer. Secondly, the irregular movement of the fluid flowing around the solo beads, which mixes the fluid more effectively. Furthermore, the metachronal wave pattern propagates along the walls of the tube. The next sections comprises of the philosophical analysis of the problem statement. The closed form exact solution for velocity, temperature and pressure gradients is presented in section 3. The physical insight of the analysis through plots and tables is presented in section 4. Last section summarizes some outcomes of the present study.

2. Problem analysis

Let us consider ciliary transport of two-dimensional, incompressible, and axisymmetric flow of a silicon dioxide water nanofluid in a finite flexible horizontal tube tube having porous medium. The inner surface of the tube is ciliated with metachronal waves and these waves are developed due to collective beating of cilia, which directs the flow. An inclined
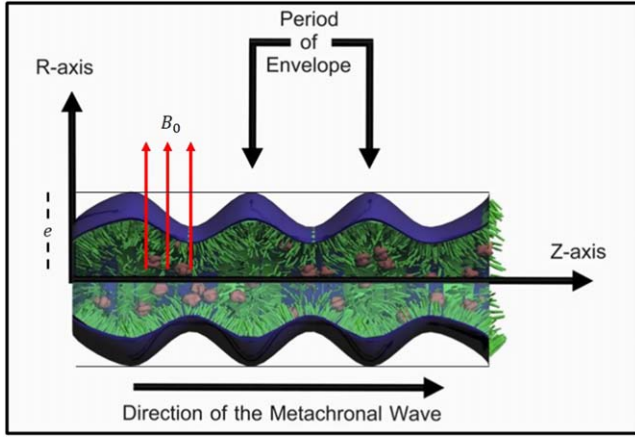
Figure 1. Geometry of the problem.

magnetic field of strength B_0 is applied in the axial direction with inclination angle (ξ). Moreover, heat transfer analysis is studied with Joule heating, viscous dissipation and internal heat source effect. Cylindrical coordinate system ($\overline{R}$, $\overline{Z}$), is selected in such a manner such that $\overline{R}$-axis is perpendicular to the tube and $\overline{Z}$-axis lies along the center of the tube. The sinusoidal wave is propagating along the walls of the channel with a wave velocity (c) and wavelength (λ). No slip condition suggests that the cilia tips and fluid adjacent to cilia tips have same velocity, so the radial and axial velocities are given as follows [17]:

$$\overline{U} = \frac{\left(\frac{2\pi}{\lambda}\right)\left[ce\epsilon\alpha\sin\left(\frac{2\pi}{\lambda}(\overline{Z} - c\overline{t})\right)\right]}{1 - \frac{2\pi}{\lambda}\left[e\epsilon\alpha\cos\left(\frac{2\pi}{\lambda}(\overline{Z} - c\overline{t})\right)\right]},$$

$$\overline{W} = \frac{\left(\frac{-2\pi}{\lambda}\right)\left[ce\epsilon\alpha\cos\left(\frac{2\pi}{\lambda}(\overline{Z} - c\overline{t})\right)\right]}{1 - \frac{2\pi}{\lambda}\left[e\epsilon\alpha\cos\left(\frac{2\pi}{\lambda}(\overline{Z} - c\overline{t})\right)\right]}. \tag{1}$$

Figure 1 provides the schematic picture of the assumed model and the coordinate system.

　　Making use of following transformation to convert the flow from fixed frame to wave frame.

$$\overline{R} = \overline{r}, \ \overline{U} = \overline{u}, \ \overline{Z} = \overline{z} + c\overline{t},$$
$$\overline{W} = \overline{w} + c, \ \overline{p}(\overline{z}, \overline{r}) = \overline{P}(\overline{Z}, \overline{R}, \overline{T}). \tag{2}$$

The fundamental governing equations in the fixed frame is given as [23]:

$$\frac{\partial\overline{u}}{\partial\overline{r}} + \frac{\overline{u}}{r} + \frac{\partial\overline{w}}{\partial\overline{z}} = 0, \tag{3}$$

$$\rho_{nf}\left[\overline{u}\frac{\partial\overline{u}}{\partial\overline{r}} + \overline{w}\frac{\partial\overline{u}}{\partial\overline{z}}\right] = -\frac{\partial\overline{p}}{\partial\overline{r}} + 2\mu_{nf}\left[\frac{\partial^2\overline{u}}{\partial\overline{r}^2} + \frac{1}{r}\frac{\partial\overline{u}}{\partial\overline{r}} - \frac{\overline{u}}{r^2}\right]$$
$$+ \mu_{nf}\left[\frac{\partial^2\overline{w}}{\partial\overline{z}^2} + \frac{\partial^2\overline{u}}{\partial\overline{z}\partial\overline{r}}\right], \tag{4}$$

Table 1. Thermophysical properties of silicon dioxide and water.

Item	$\rho(\text{kg m}^{-3})$	$c_p(\text{J kg}^{-1}\,\text{K}^{-1})$	$K(\text{W mk}^{-1})$
SiO_2	2220	680	1.38
H_2O	999	4 179.0	0.615

$$\rho_{nf}\left[\overline{u}\frac{\partial\overline{w}}{\partial\overline{r}} + \overline{w}\frac{\partial\overline{w}}{\partial\overline{z}}\right] = -\frac{\partial\overline{p}}{\partial\overline{z}} + 2\mu_{nf}\left[\frac{\partial^2\overline{w}}{\partial\overline{z}^2}\right]$$
$$+ \mu_{nf}\left[\frac{1}{r}\left(\frac{\partial\overline{u}}{\partial\overline{z}} + \frac{\partial\overline{w}}{\partial\overline{r}}\right) + \frac{\partial}{\partial\overline{r}}\left(\frac{\partial\overline{u}}{\partial\overline{z}} + \frac{\partial\overline{w}}{\partial\overline{r}}\right)\right]$$
$$- \sigma_{bf}B_0^2\cos(\xi)(\overline{w} + c) - \frac{\mu_{nf}}{K}(\overline{w} + c), \tag{5}$$

$$(\rho c_p)_{nf}\left[\overline{u}\frac{\partial\overline{T}}{\partial\overline{r}} + \overline{w}\frac{\partial\overline{T}}{\partial\overline{z}}\right] = k_{nf}\left[\frac{\partial^2\overline{T}}{\partial\overline{z}^2} + \frac{1}{r}\frac{\partial}{\partial\overline{r}}\left(\overline{r}\frac{\partial\overline{T}}{\partial\overline{r}}\right)\right]$$
$$+ Q_0 + \sigma_{bf}B_0^2\cos(\xi)(\overline{w} + c)^2$$
$$+ \mu_{nf}\left[2\left(\frac{\partial\overline{u}}{\partial\overline{z}}\right)^2 + 2\left(\frac{\partial\overline{w}}{\partial\overline{r}}\right)^2 + \left(\frac{\partial\overline{u}}{\partial\overline{r}} + \frac{\partial\overline{w}}{\partial\overline{z}}\right)^2\right]. \tag{6}$$

The suitable boundary conditions on wall are:

$$\frac{\partial\overline{w}}{\partial\overline{r}} = 0, \ \frac{\partial\theta}{\partial r} = 0,$$
$$\text{at} \quad r = 0, \tag{7}$$

$$\overline{w} = \frac{-2\pi\epsilon\alpha\beta\cos(2\pi z)}{1 - 2\pi\epsilon\alpha\beta\cos(2\pi z)} - 1,$$
$$\theta = 0 \ at \ r = \hbar(z), \tag{8}$$

here $\overline{u}$ and $\overline{w}$ are the velocity elements in the radial $\overline{r}$ and axial $\overline{z}$ directions, respectively, where σ_{bf} the electrical conductivity, ξ the inclination angle, $\overline{T}$ the fluid temperature, Q_0 the internal heat source coefficient, K the permeability parameter. As this analysis incorporates irregular particle geometries by introducing a shape factor, therefore Hamilton and Crosser model [44] is taken into consideration. According to this model, the thermal conductivity can be expressed as:

$$\alpha_{nf} = \frac{k_{nf}}{(\rho c_p)_{nf}}, \ (\rho c_p)_{nf} = (1 - \phi)(\rho c_p)_{bf} + \phi(\rho c_p)_p,$$
$$\mu_{nf} = \frac{\mu_{bf}}{(1 - \phi)^{2.5}},$$
$$\rho_{nf} = (1 - \phi)\rho_{bf} + \phi\rho_{bf},$$
$$k_{nf} = \frac{k_p + (m + 1)k_{bf} - (m + 1)(k_{bf} - k_p)\phi}{k_p + (m + 1)k_{bf} + (k_{bf} - k_p)\phi}k_{bf}, \tag{9}$$

where the subscripts p, nf and bp represents the solid nanoparticles, nanofluid and base fluid, respectively and α_{nf} shows the effective thermal diffusivity, ρc_p the heat capacitance, μ_{nf} the effective dynamic viscosity, ρ_{nf} the effective density, m the shape factor and k_{nf} the effective thermal conductivity. Thermophysical properties of the base fluids and nanoparticles are presented in table 1 by Talib *et al* [6]. Table 2 shows the nanoparticles shape and their respective shape factor.

Table 2. Nanoparticle shapes with their shape factor is given by Elena et al [45].

Nanoparticles	Shape	Shape Factor
Bricks		3.70
Cylinders		4.90
Platelets		5.70

Introducing the following non-dimensional variables.

$$
\left.\begin{array}{l}
z = \dfrac{\overline{z}}{\lambda}, \ \ r = \dfrac{\overline{r}}{e}, \ \ u = \dfrac{\lambda \overline{u}}{ec}, \ \ \delta = \dfrac{e}{\lambda}, \\[2mm]
h = \dfrac{\hbar}{e} = 1 + \epsilon \cos(2\pi z), \\[2mm]
Re = \dfrac{ec\rho_{\mathrm{nf}}}{\mu_{\mathrm{bf}}}, \ \ w = \dfrac{\overline{w}}{c}, \ \ p = \dfrac{e^2 \overline{p}}{c\lambda \mu_{\mathrm{bf}}}, \\[2mm]
Br = \dfrac{c^2 \mu_{\mathrm{bf}}}{k_{\mathrm{bf}} \overline{T_0}}, \ \ \Omega = \dfrac{Q_0 e^2}{k_{\mathrm{bf}} \overline{T_0}}, \\[2mm]
\theta = \dfrac{(\overline{T} - \overline{T_0})}{\overline{T_0}}, \ \ Ha^2 = \dfrac{e^2 B_0^2 \sigma_{\mathrm{bf}}}{\mu_{\mathrm{bf}}}, \\[2mm]
Da = \dfrac{K}{e^2}, \ \ J_h = \dfrac{\sigma_{\mathrm{bf}} c^2 e^2}{k_{\mathrm{bf}} T_0} B_0^2.
\end{array}\right\} \quad (10)
$$

By considering the above non-dimensional variables in equations (3)–(8) and the limitations of creeping flow are enforced, i.e. inertial forces are minute as compared to viscous forces, therefore a very low Reynolds number ($Re \ll 1$) is considered. Also the metachronal wave wavelength is assumed to be very large (i.e. $\lambda \to \infty$).

The reduced set of ordinary differential equations are:

$$
\frac{\mathrm{d}p}{\mathrm{d}r} = 0, \quad (11)
$$

$$
\frac{\mathrm{d}p}{\mathrm{d}z} - \frac{1}{(1-\phi)^{2.5}}\left(\frac{1}{r}\frac{\mathrm{d}w}{\mathrm{d}r} + \frac{\mathrm{d}^2 w}{\mathrm{d}r^2}\right)
$$
$$
+ \left(Ha^2 \cos(\xi) + \frac{1}{(1-\phi)^{2.5}}\frac{1}{Da}\right)(w+1) = 0, \quad (12)
$$

$$
\Psi_1\left(\frac{\mathrm{d}^2 \theta}{\mathrm{d}r^2} + \frac{1}{r}\frac{\mathrm{d}\theta}{\mathrm{d}r}\right)
$$
$$
+ \frac{Br}{(1-\phi)^{2.5}}\left(\frac{\mathrm{d}w}{\mathrm{d}r}\right)^2 + J_h \cos(\xi)(w+1)^2 + \Omega = 0, \quad (13)
$$

where

$$
\Psi_1 = \frac{k_p + (m+1)k_{\mathrm{bf}} - (m+1)(k_{\mathrm{bf}} - k_p)\phi}{k_p + (m+1)k_{\mathrm{bf}} + (k_{\mathrm{bf}} - k_p)\phi}, \quad (14)
$$

where Ha is the Hartmann number, Br the Brinkman number, J_h the Joule heating parameter, Da the Darcy number and Ω the heat source parameter. The suitable boundary conditions on the walls are:

$$
\frac{\mathrm{d}w}{\mathrm{d}r} = 0, \ \ \frac{\mathrm{d}\theta}{\mathrm{d}r} = 0, \ \ \text{at} \ \ r = 0, \quad (15)
$$

$$
w = \frac{-2\pi\epsilon\alpha\beta\cos(2\pi z)}{1 - 2\pi\epsilon\alpha\beta\cos(2\pi z)} - 1,
$$
$$
\theta = 0 \ \ \text{at} \ \ r = \hbar(z) = 1 + \epsilon\cos(2\pi z). \quad (16)
$$

The volumetric entropy generation term S_{Gen} can be calculated as follows [23]:

$$
S_{\mathrm{Gen}} = \frac{k_{\mathrm{nf}}}{\theta_0^2}\left(\left(\frac{\partial \overline{T}}{\partial \overline{r}}\right)^2 + \left(\frac{\partial \overline{T}}{\partial \overline{z}}\right)^2\right)
$$
$$
+ \frac{\mu_{\mathrm{nf}}}{\overline{\theta_0}}\left[2\left(\frac{\partial \overline{u}}{\partial \overline{z}}\right)^2 + 2\left(\frac{\partial \overline{w}}{\partial \overline{r}}\right)^2 + \left(\frac{\partial^2 \overline{u}}{\partial \overline{r}} + \frac{\partial^2 \overline{w}}{\partial \overline{z}}\right)^2\right]
$$
$$
+ \frac{\sigma_{\mathrm{bf}} B_0^2}{\overline{\theta_0}}\cos(\xi)(\overline{w} + c)^2, \quad (17)
$$

the rate of dimensionless entropy formation $\left(E_G = \frac{S_{\mathrm{Gen}}}{S_{\mathrm{gen}}}\right)$ is:

$$
E_G = \Psi_1\left(\frac{\mathrm{d}\theta}{\mathrm{d}r}\right)^2 + \frac{\Lambda Br}{(1-\phi)^{2.5}}\left(\frac{\mathrm{d}w}{\mathrm{d}r}\right)^2
$$
$$
+ \Lambda Br Ha^2 \cos(\xi)(w+1)^2, \quad (18)
$$

or

$$
E_G = E_H + E_V + E_M. \quad (19)
$$

Equation (17) demonstrate the three distinct roots for the entropy formation:

- 1st term appears as a result of heat transfer (E_H) irreversibility.
- 2nd term comes out due to the existence of viscous dissipation (E_V).
- 3rd term yield due to the presence the magnetic parameter (E_M).

The finite temperature difference and characteristic entropy generation are given, respectively, as:

$$
\Lambda = \frac{\overline{\theta_0}}{\overline{T_0}}, \ \ S_{\mathrm{gen}} = \frac{k_{\mathrm{bf}}\overline{T_0^2}}{\theta_0^2 e_1^2}. \quad (20)
$$

Now Bejan number (Be) is introduced to calculate the irreversibility distribution, which is the ratio of the heat transfer irreversibility to total irreversibility, given as:

$$
Be = \frac{E_H}{E_H + E_V + E_M}. \quad (21)
$$

3. Exact solutions

This segment presents the closed form exact solutions to the ordinary differential equations (12) and (13)together with the
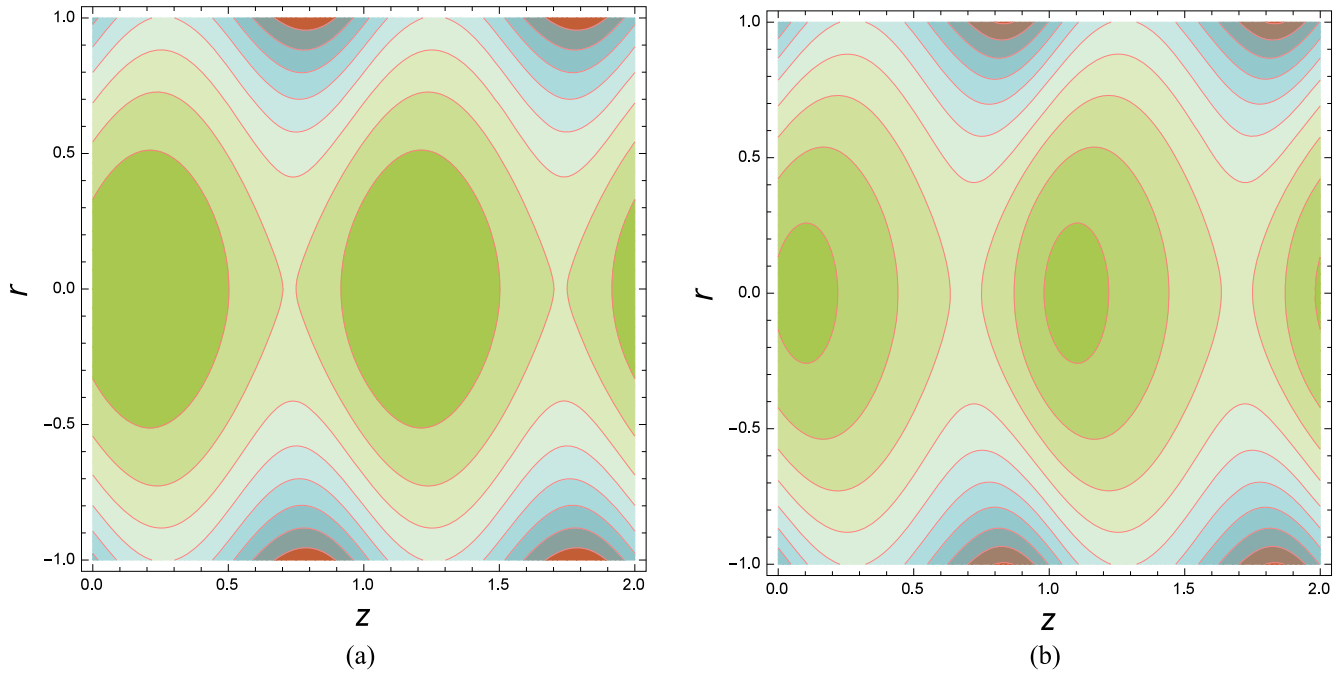
(a)

(b)

Figure 2. (a) Streamlines for $\alpha = 0.2$. (b) Streamlines for $\alpha = 0.5$.
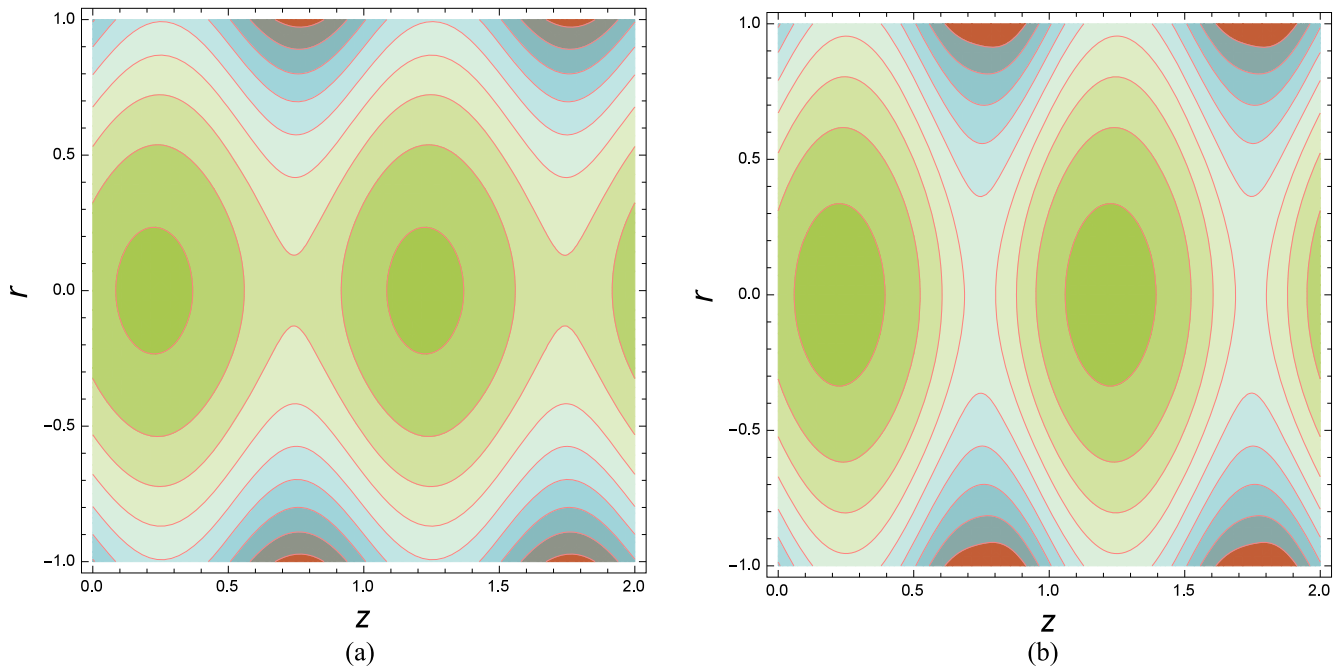

(a)

(b)

Figure 3. (a) Streamlines for $\epsilon = 0.2$. (b) Streamlines for $\epsilon = 0.3$.

boundary conditions (15) and (16). The constitutive boundary layer equations for the considered flow analysis incorporates continuity, momentum and energy equations. These equations are coupled nonlinear partial differential equations. To convert the governing system of partial differential equations to system of ordinary differential equations, similarity variables have been introduced. The obtained system is a linear, 2nd order inhomogeneous ordinary differential system. The exact solution of ordinary differential system presented in equations (22), (24)

and (25) is acquired by the program designed in the MATHEMATICA software called 'DSolve'. The general solution of inhomogeneous differential equations comprises of the complementary and particular parts. For complementary solution, 'DSolve' chooses the Bessel functions, because the homogeneous part of equations (12) and (13)corresponds to the standard form of Bessel equation of order zero. Once we are successful in obtaining the complementary solution, 'DSolve' straightforwardly proceeds for the particular solution

$$w(r, z) = \frac{-\Psi_2 J_0[h\Psi_3]\left(1 + Da\frac{dp}{dz} + DaHa^2\cos(\xi)\right) + J_0[rh\Psi_3](-1 + \Psi_4\cos(\xi))}{\Psi_2 J_0[h\Psi_3](1 + DaHa^2\cos(\xi))}, \tag{22}$$

whereas the flow rate is given by

$$Q = 2\int_0^{\hbar(z)} rw(r, z)dr, \tag{23}$$

now substituting equation (22) into equation (23) and then we have solution of dp/dz

$$\frac{dp}{dz} = \frac{4\left(-\Psi_2(F + h^2)\,{}_0F_1\left[\frac{h^2\Psi_3\sqrt{(1 - \phi)^{2.5}}}{4}\right] + h^2(\Psi_2 - 1)\,{}_0F_2\left[\frac{h^2\Psi_3\sqrt{(1 - \phi)^{2.5}}}{4}\right]\right)}{h^4\Psi_2(1 - \phi)^{2.5}\,{}_0F_3\left[\frac{h^2\Psi_3\sqrt{(1 - \phi)^{2.5}}}{4}\right]}, \tag{24}$$

$$\theta(r, z) = \frac{(h - r)(h + r)(\Psi_5^2 Br + \Omega(1 - \phi)^{2.5}) + (1 + \Psi_6)^2 J_h(1 - \phi)^{2.5}\cos(\xi)}{4\Psi_2(1 - \phi)^{2.5}}, \tag{25}$$

where the expressions for $(\Psi_i, i = 2 - 6)$ are given as:

$$\left.\begin{aligned}
\Psi_2 &= \frac{-2\pi\epsilon\alpha\beta\cos(2\pi z)}{1 - 2\pi\epsilon\alpha\beta\cos(2\pi z)} - 1,\\[6pt]
\Psi_3 &= ((1 - \phi)^{2.5})^{1/2}\sqrt{\frac{1}{Da} + Ha^2\cos(\xi)},\\[6pt]
\Psi_4 &= \Psi_2 + Da\Psi_2\frac{dp}{dz} + DaHa^2(-1 + \Psi_2),\\[6pt]
\Psi_5 &= -\frac{r(h^2 + F\Psi_2)\Psi_3^2\,{}_0F_2\left[\frac{r^2\Psi_3^2}{4}\right]}{2h^2\Psi_2 I_1\left[h\sqrt{(1 - \phi)^{2.5}\left(\frac{1}{Da} + Ha^2\cos(\xi)\right)}\right]},\\[6pt]
\Psi_6 &= \frac{\left(\Psi_2 F\,{}_0F_1\left[\frac{h^2\Psi_3^2}{4}\right] - (h^2 + F\Psi_2)\,{}_0F_1\left[\frac{r^2\Psi_3^2}{4}\right] + h^2\,{}_0F_2\left[\frac{h^2\Psi_3^2}{4}\right]\right)}{h^2\Psi_2 I_2\left[h\sqrt{(1 - \phi)^{2.5}\left(\frac{1}{Da} + Ha^2\cos(\xi)\right)}\right]}
\end{aligned}\right\} \tag{26}$$

where the mean flow rate is equal to:

$$F = Q - \left[0.5 + \frac{\epsilon^2}{4}\right], \tag{27}$$

Table 3 provides the validation of our code and this validation is made on the basis of comparison table with already published article. The local Nusselt number is given as.

$$Nu = -\left(\frac{\partial\theta}{\partial r}\right)_{r=h}. \tag{28}$$

4. Results and discussion

This section is developed to discuss the physical influence of various pertinent parameters on streamlines, velocity field, pressure gradient and temperature field with the impact of two different shaped nanoparticles respectively. For this purpose streamlines are plotted against the eccentricity of elliptical motion (α) and wave amplitude (ϵ). It is clear from figures 2(a), (b) that with an increase in the magnitude of eccentricity elliptical motion the size of bolus decreases and number of trapped bolus increases. Figures 3(a), (b) shows that by enlarging the wave amplitude both the size and number of trapped bolus increases. The influence of Hartmann number (*Ha*) for both pure fluid and nanofluid with combine effect of low (*Da* = 0.05) and high (*Da* = 5.0) Darcy number against $w(r, z)$ is plotted in figures 4(a), (b) respectively. It is found that as *Ha* increases there is gradual decrease in the fluid velocity. Physically, an increasing in the
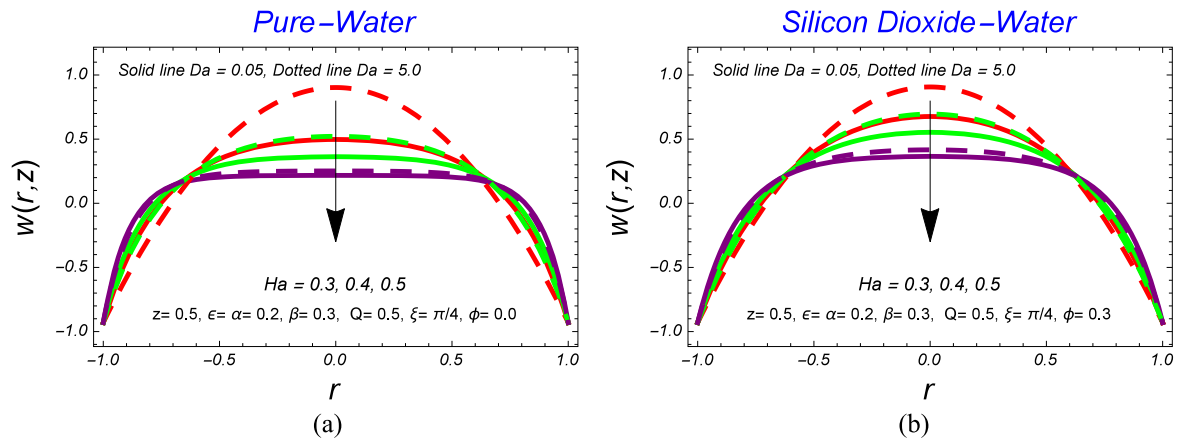
Figure 4. (a) Variation of *Ha* at $w(r, z)$ with multiple values of *Da*. (b) Variation of *Ha* at $w(r, z)$ with multiple values of *Da*.
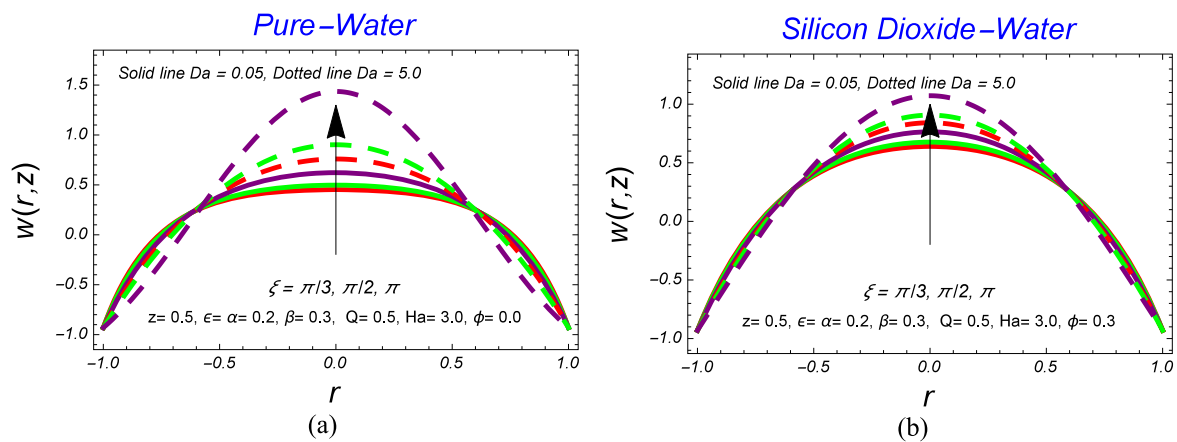

Figure 5. (a) Variation of ξ at $w(r, z)$ with multiple values of *Da*. (b) Variation of ξ at $w(r, z)$ with multiple values of *Da*.
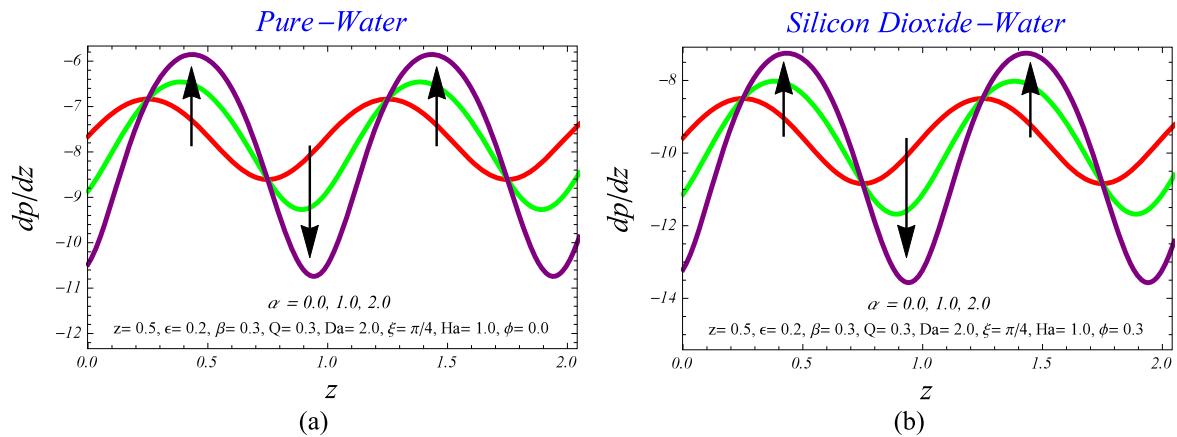

Figure 6. (a) Variation of α at dp/dz for pure and diluted water. (b) Variation of α at dp/dz for pure and diluted water.

magnetic field enhances the Lorentz force, which is a resistive force, therefore more resistance is offered to the fluid motion which consequently reduces the velocity. The variation of inclination angle (ξ) against $w(r, z)$ is plotted in figures 5(a), (b) respectively. It is seen that by increasing the inclination angle the fluid velocity increases significantly. It is also noticed that the fluid velocity is huge in case of pure fluid as compared to nanofluid see figures 4(a), (b) and 5(a), (b).

Figures 6(a), (b) shows the influence of α on pressure gradient (dp/dz) against the axial direction. The pressure gradient is a physical quantity that characterize in which direction and at what rate the pressure raises the most rapidly. Figures 6(a), (b) shows a non-uniform oscillating behavior for increasing values of α. Also more pressure gradient is offered by pure fluid as compared to the diluted fluid. Figure 7(a) depicts the influence of effective thermal conductivity of
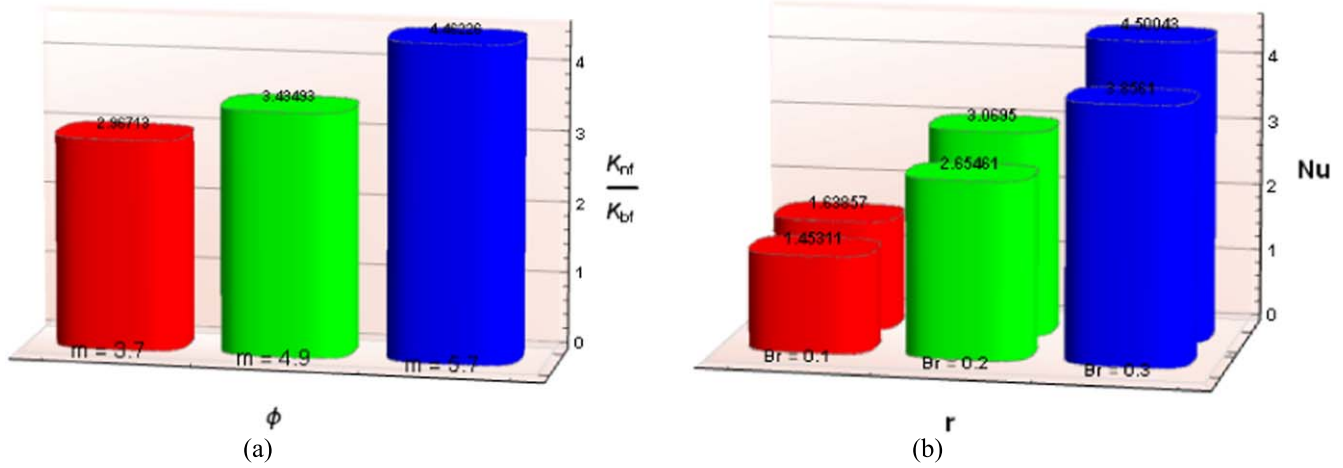
Figure 7. (a) Variation of K_{nf}/K_{bf} to ϕ for different m. (b) Variation of Br to r with $\phi = 0.0$ and $\phi = 0.1$.
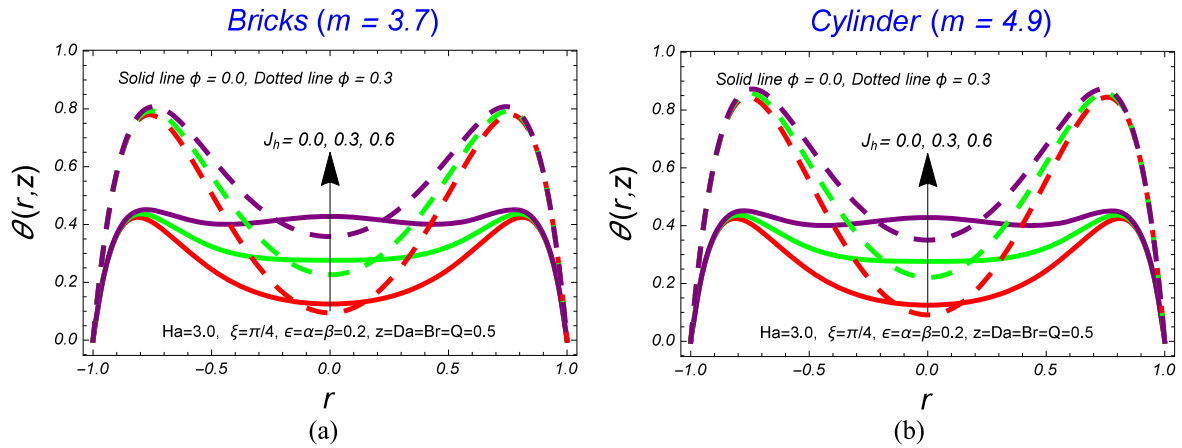

Figure 8. (a) Variation of J_h at $\theta(r, z)$ for pure and diluted water. (b) Variation of J_h at $\theta(r, z)$ for pure and diluted water.
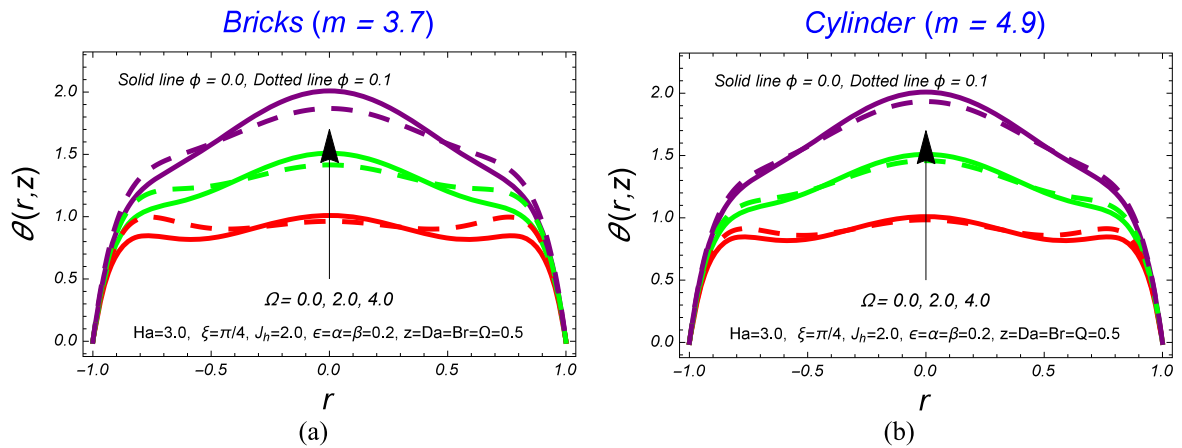

Figure 9. (a) Variation of Ω at $\theta(r, z)$ for pure and diluted water. (b) Variation of Ω at $\theta(r, z)$ for pure and diluted water

nanofluid against the three distinct shapes of the nano-particles. We can clearly see a meaningful variation in the thermal conductivities of these nanoparticles, where the Pla-telets having the maximum and Bricks having the minimum thermal conductivity. Note that the solid nanoparticle volume fraction is directly proportional to the thermal conductivity of the fluid. The higher the solid nanoparticle fraction the greater the thermal conductivity of the fluid see [16]. Figure 7(b) shows the influence of Brinkman number on Nusselt number while keeping $\phi = 0.0$ and $\phi = 0.1$. It is examined that for
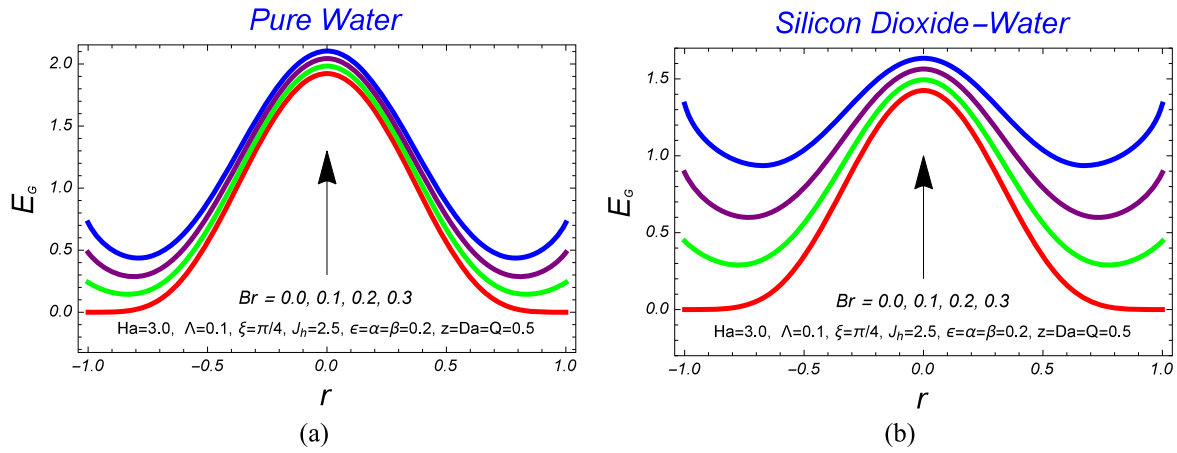
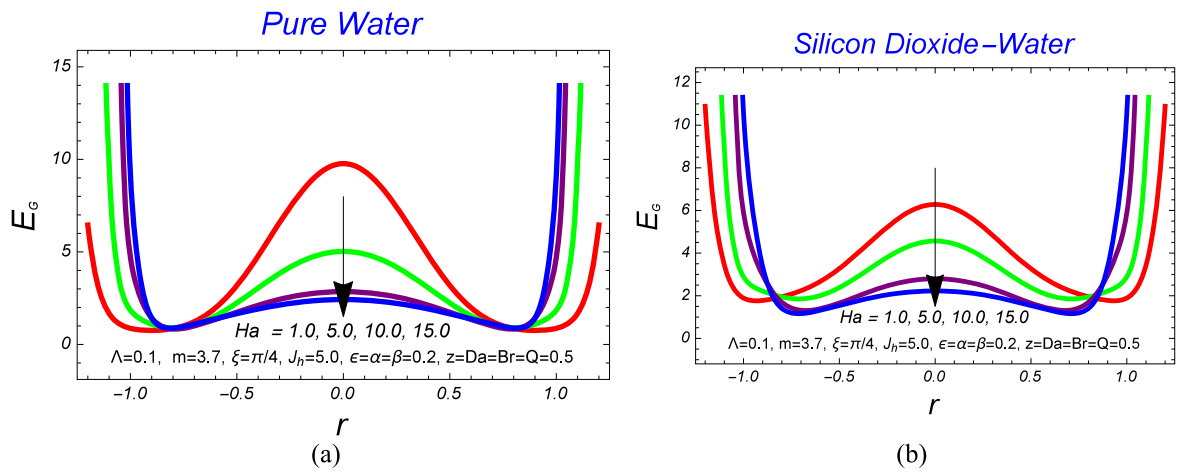**Figure 10.** (a) Response of *Br* at E_G for pure water. (b) Response of *Br* at E_G for diluted water.

Figure 11. (a) Response of *Ha* at E_G for pure water. (b) Response of *Ha* at E_G for diluted water.
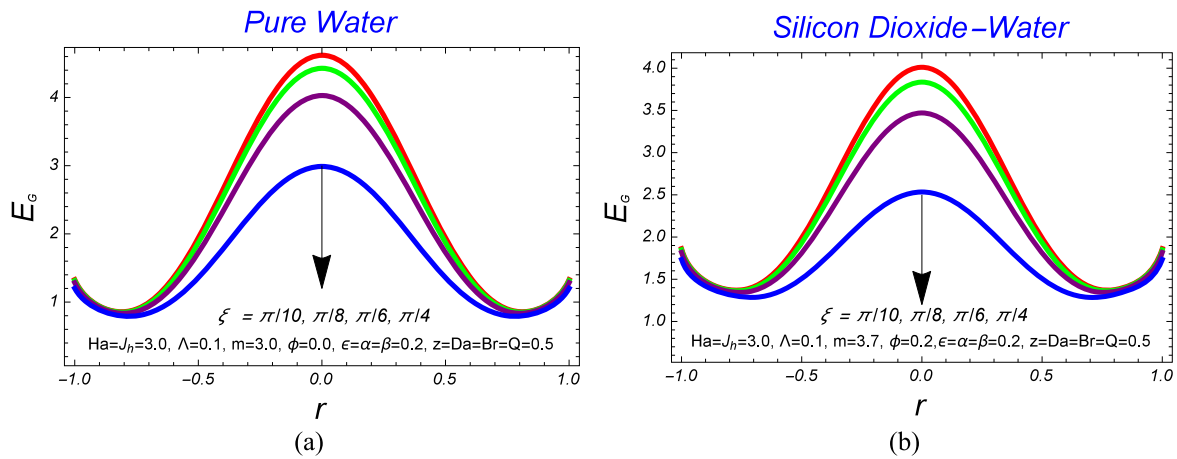

Figure 12. (a) Response of ξ at E_G for pure water. (b) Response of ξ at E_G for diluted water.

increasing values of Brinkman number the rate of heat transfer increases, but the heat transfer rate gets more accelerated by increasing the nanoparticle concentration from 0 to 0.1 with an increment in Brinkman parameter. The impact of Joule heating (J_h) and internal heat source parameter (Ω) with shaped nanoparticles (i.e. Bricks and Cylinders) on $\theta(r, z)$ is

graphed in figures 8(a), (b) and 9(a), (b). We can see that as the magnitude of Joule heating parameter increases there is an increase in the temperature profile. Physically, due to inside friction of molecules, the mechanical energy converted into thermal energy is responsible for temperature enhancement. Furthermore, the fluid temperature is maximum near the
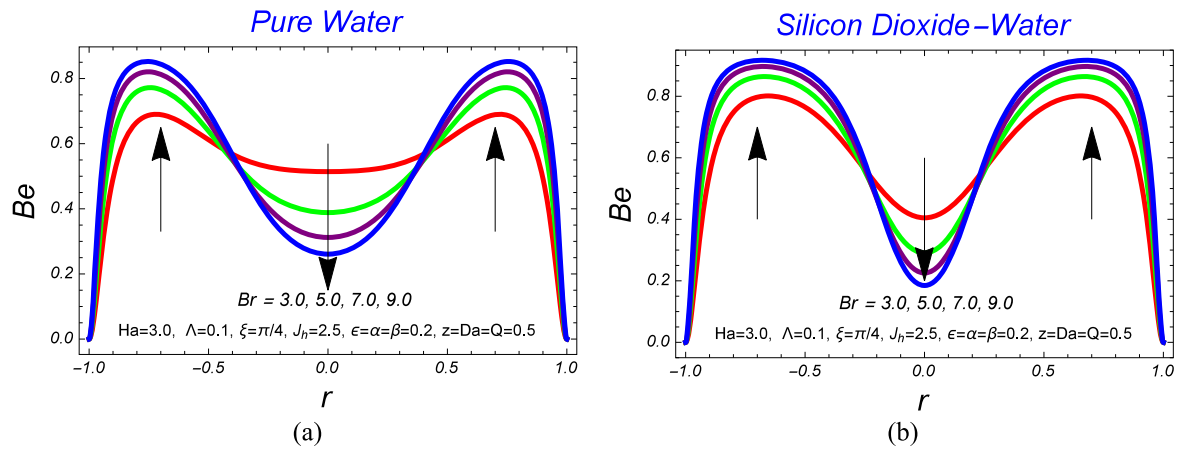
Pure Water

Silicon Dioxide–Water

Figure 13. (a) Response of *Br* at *Be* for pure water. (b) Response of *Br* at *Be* for diluted water.

Pure Water

Silicon Dioxide–Water

Figure 14. (a) Response of *Ha* at *Be* for pure water. (b) Response of *Ha* at *Be* for diluted water.

Pure Water
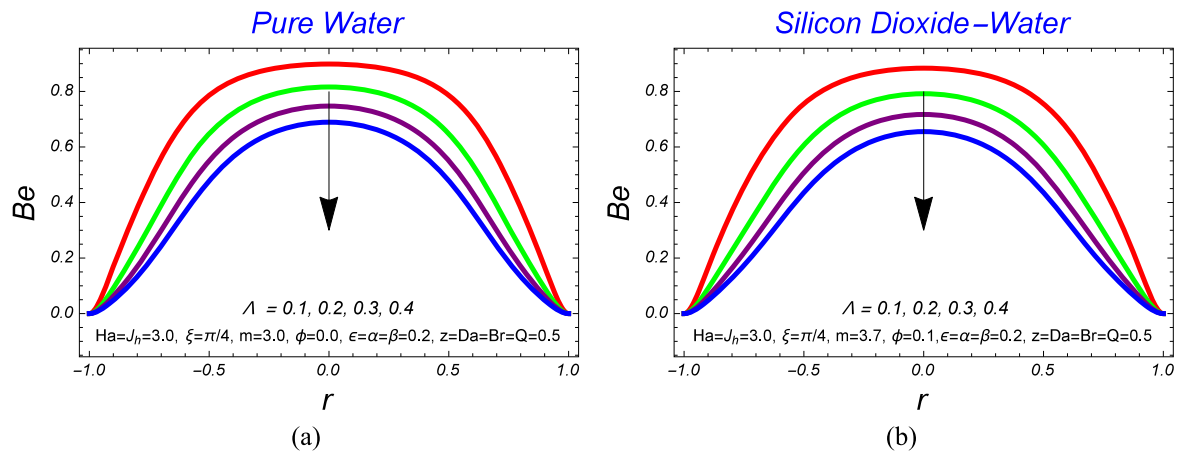

Silicon Dioxide–Water

Figure 15. (a) Response of Λ at *Be* for pure water. (b) Response of Λ at *Be* for diluted water.

ciliated walls and least at the center of the duct see figures 8(a), (b). Figures 9(a), (b) shows that temperature field is the increasing function of Ω.

4.1. Second law analysis

In this section, multiple plots have been presented to reflect the Variation of pertinent parameters on the entropy.

Figures 10(a), (b) shows that the entropy of the fluid system increases with an increase in the magnitude of the Brinkman number (*Br*). As *Br* increases, heat transfer influence fluid viscosity within the tube, therefore increases the entropy. An enhancement in the Hartmann number (*Ha*) reduces the entropy at the center of the duct, whereas in the vicinity of the cilated walls, the formation of entropy increases constantly see figures 11(a), (b). Figures 12(a), (b) shows that an

Table 3. Code validation table while taking $z = 0.5$, $m = 0.0$, $J_h = 0.0$, $Br = 0.0$.

ϕ	ϵ	Ω	$\theta(r, z)$ Present solution			$\theta(r, z)$ Akbar *et al* [46]		
			$r = 0.0$	$r = 0.25$	$r = 0.5$	$r = 0.0$	$r = 0.25$	$r = 0.5$
0.01	0.5	0.3	0.030 8926	0.028 9227	0.023 011	0.030 8918	0.028 9219	0.023 012
0.05			0.028 4448	0.026 465	0.020 5651	0.028 4459	0.026 476	0.020 5662
0.1			0.025 5312	0.023 5613	0.017 6514	0.025 5304	0.023 5605	0.017 6507
	0.1		0.005 106 15	0.004 712 14	0.003 530 24	0.005 106 08	0.004 712 09	0.003 530 13
	0.2		0.010 2133	0.009 424 28	0.007 060 27	0.010 2122	0.009 424 19	0.007 060 26
	0.3		0.015 3178	0.014 1356	0.010 5915	0.015 3182	0.014 1363	0.010 5904
		0.0	0.060 75	0.056 0625	0.042	0.060 75	0.056 0625	0.042
		0.1	0.040 5745	0.037 4457	0.028 0521	0.040 5774	0.037 4464	0.028 0535
		0.2	0.026 1456	0.024 1345	0.018 0723	0.026 1495	0.024 1318	0.018 0787

increase in inclination angle (ξ) reduces the entropy production over all. Maximum entropy is seen at the bottom of the duct and least entropy is seen near the ciliated walls in all cases. Further, high entropy of the fluid system is seen in all cases of pure fluid, while water based silicon dioxide nanofluid have minimum entropy (see figures 10–12).

Figures 13–15 are portrayed to analyze the nature of Bejan number (*Be*) against the raidal distance under the variations in various physical parameters involved in the model. Figures 13(a), (b) shows that an increase in the *Br* causes to reduce the Bejan number at the center of the duct, whereas in the vicinity of the cilated walls, the Bejan number increases. Figures 14(a), (b) and 15(a), (b) depicts that *Be* is inversely proportional to Hartmann number and dimensionless temperature.

5. Conclusion

The considered flow analysis leads to the following meaningful conclusion:

- With an increase in the eccentricity of elliptical motion the size of bolus reduces and the number of trapped bolus increases.
- It is seen that increasing magnitude of Hartmann number reduces the flow velocity.
- It is seen that higher magnitude of Joule heating and internal heat source parameter increases the temperature of the fluid significantly.
- The local Nusselt number boost with an enhancement in Brinkman number along with increase of nanoparticle concentration.
- It is seen from 3D bar graphs that Platelets have maximum thermal conductivity and Bricks hold least.
- It is examined that as nanoparticles changes from Bricks to Cylinders the temperature of the fluid increases significantly.

- The solid nanoparticle volume fraction is directly proportional to the thermal conductivity of the fluid. The higher the solid nanoparticle fraction the greater the thermal conductivity of the fluid.
- It is found that entropy is directly proportional to Brinkmann number and inversely proportional inclination angle.
- Bejan number is the decreasing function of Hartmann number and dimensionless temperature difference.

References

[1] Choi S U S 1995 Enhancing thermal conductivity of fluids with nanoparticle *Developments and Applications of Non-Newtonian Flows* ed D A Siginer and H P Wang (United States: Argonne National Lab., IL) pp 99–105 ASME FED, 231/ MD- 66

[2] Dobson J 2006 Magnetic nanoparticles for drug delivery *Drug Dev. Res.* **67** 55–60

[3] Hadjipanayis C G, Machaidze R, Kaluzova M, Wang L, Schuette A J, Chen H, Wu X and Mao H 2010 EGFRvIII antibody conjugated iron oxide nanoparticles for magnetic resonance imaging guided convection-enhanced delivery and targeted therapy of glioblastoma *Cancer Res.* **70** 6303–12

[4] Girginova P I, Daniel-de-Silva A L, Lopes C B, Figueira P, Otero M, Amaral V S, Pereira E and Trindade T 2010 Silica coated magnetite particles for magnetic removal of Hg^{+2} from water *J. Colloid Interface Sci.* **345** 234–40

[5] Kulkarni D P, Namburu P K, Bargar H E D and Das D K 2008 Convective heat transfer and fluid dynamic characteristics of SiO_2 -ethylene glycol/water nanofluid *Heat Transfer Eng.* **29** 1027–35

[6] Talib S F A, Azmi W H, Zakaria I, Mohamed W, Mamat A M I, Ismail H and Daud W R W 2015 Thermophysical properties of silicon dioxide (SiO_2) in ethylene glycol/water mixture for proton exchange membrane fuel cell cooling application *Energy Proc.* **79** 366–71

[7] Yan S, Wang F, Shi Z G and Tian R 2017 Heat transfer property of (SiO_2)/water nanofluid flow inside solar collector vacuum tubes *Appl. Therm. Eng.* **118** 385–91

[8] Abrar M N and Awais M 2018 Rheology of alumina and silver nanoparticles over an exponentially stretching convective wall *J. Comput. Theor. Nanosci.* **15** 1373–8

[9] Estellé P, Halelfadl S and Mare T 2016 Thermophysical properties and heat transfer performance of carbon nanotubes water-based nanofluids *J. Therm. Anal. Calorim.* **127** 2075–81

[10] Abrar M N, Sagheer M and Huassain S 2019 Entropy analysis of SWCNT & MWCNT flow induced by collecting beating of cilia with porous medium *J. Cent. South Univ.* **26** 2109–18

[11] Turkyilmazoglu M and Pop I 2013 Heat and mass transfer of unsteady natural convection flow of some nanofluids past a vertical infinite flat plate with radiation effect *Int. J. Heat Mass Transfer.* **59** 167–71

[12] Hussain S, Öztop H F, Jamal M and Hamdeh N A 2017 Double diffusive nanofluid flow in a duct with cavity heated from below *Int. J. Mech. Sci.* **131** 535–45

[13] Garoosi F, Bagheri G and Talebi F 2013 Numerical simulation of natural convection of nanofluids in a square cavity with several pairs of heaters and coolers (HACs) inside *Int. J. Heat Mass Transfer* **67** 362–76

[14] Nield D and Kuznetsov A 2013 The onset of convection in an internally heated nanofluid layer *J. Heat Transfer* **136** 014501

[15] Sheikholeslami M, Rashidi M M and Ganji D D 2015 Numerical investigation of magnetic nanofluid forced convective heat transfer in existence of variable magnetic field using two phase model *J. Mol. Liq.* **212** 117–26

[16] Akbar N S and Butt A W 2015 Ferromagnetic effects for peristaltic flow of Cu-water nanofluid for different shapes of nanosize particles *Appl. Nanosci.* **6** 379–85

[17] Abrar M N, Sagheer M and Huassain S 2018 Entropy analysis of Hall current and thermal radiation influenced by cilia with single and multi wall carbon nanotubes *Bull. Mater. Sci.* **42** 250–60

[18] Avramenko A A, Blinov D G and Shevchuk I V 2011 Self-similar analysis of fluid flow and heat-mass transfer of nanofluids in boundary layer *Phys. Fluids* **23** 082002

[19] Yadav D 2014 *Hydrodynamic and Hydromagnetic Instability in Nanofluids* (Germany: Lambert Academic Publishing)

[20] Rana G C, Thakur R C and Kango S K 2014 On the onset of double-diffusive convection in a layer of nanofluid under rotation saturating a porous medium *J. Porous Media* **17** 657–67

[21] Yadav D and Lee J 2015 The effect of local thermal non-equilibrium on the onset of Brinkman convection in a nanofluid saturated rotating porous layer *J. Nanofluids* **4** 335–42

[22] Ali A O, Makinde O D and Gyekye Y N 2016 Numerical study of unsteady MHD Couette flow and heat transfer of nanofluids in a rotating system with convective cooling *Int. J. Numer. Methods Heat Fluid Flow* **26** 1567–79

[23] Abrar M N, Sagheer M and Huassain S 2019 Entropy formation analysis for the peristaltic motion of ferrofluids in the presence of Joule heating and fluid friction phenomena in a plumb duct *J. Nanofluids* **8** 1305–13

[24] Hamzah N S B A, Kandasamy R and Muhammad R 2016 Thermal radiation energy on squeezed MHD flow of Cu, Al_2O_3 and CNTs-nanofluid over a sensor surface *Alexandria Eng. J.* **55** 2405–21

[25] Sheremet M A, Öztop H F and Pop I 2016 MHD natural convection in an inclined wavy cavity with corner heater filled with a nanofluid *J. Magn. Magn. Mater.* **416** 37–47

[26] Sheremet M A, Pop I, Öztop H and Abu-Hamdeh N 2017 Natural convection of nanofluid inside a wavy cavity with a non-uniform heating *Int. J. Numer. Methods Heat Fluid Flow* **27** 958–80

[27] Alam M S, Ali M, Alim M A and Haque Munshi M J 2017 Unsteady boundary layer nanofluid flow and heat transfer along a porous stretching surface with magnetic field *AIP Conf. Proc.* **1851** 020023

[28] Yadav D 2019 The effect of pulsating through flow on the onset of magneto convection in a layer of nanofluid confined within a Hele–Shaw cell *J. Proc. Mech. Eng.* (https://doi.org/10.1177/0954408919836362)

[29] Yadav D 2019 The onset of longitudinal convective rolls in a porous medium saturated by a nanofluid with non-uniform internal heating and chemical reaction *J. Therm. Anal. Calorim.* **135** 1107–17

[30] Sheikholeslami M, Mehryan S A M, Shafee A and Sheremet M A 2019 Variable magnetic forces impact on magnetizable hybrid nanofluid heat transfer through a circular cavity *J. Mol. Liq.* **277** 388–96

[31] Bejan A 1979 A study of entropy generation in fundamental convective heat transfer *J. Heat Transfer* **101** 718–25

[32] Makinde O D and Gbolagade A W 2005 Second law analysis of incompressible viscous flow through an inclined channel with isothermal walls *Rom. J. Phys.* **50** 9–10

[33] Aksoy Y 2016 Effects of couple stresses on the heat transfer and entropy generation rates for a flow between parallel plates with constant heat flux *Int. J. Therm. Sci.* **107** 1–12

[34] Rashidi M M, Parsab A B, Anwar Beg O, Shamekhib L, Sadri S M and Bég A 2014 Parametric analysis of entropy generation in magneto-hemodynamic flow in a semi-porous channel with OHAM and DTM¹, Appl *Bionics Biomech.* **11** 47–60

[35] Hussain S, Ahmed S E and Akbar T 2017 Entropy generation analysis in MHD mixed convection of hybrid nanofluid in an open cavity with a horizontal channel containing an adiabatic obstacle *Int. J. Heat Mass Transfer* **114** 1054–66

[36] Kamran A, Hussain S, Sagheer M and Akmal N 2017 A numerical study of magnetohydrodynamics flow in Casson nanofluid combined with Joule heating and slip boundary conditions *Results Phys.* **7** 3037–48

[37] Abrar M N, Rizwan Ul Haq, Awais M and Rashid I 2017 Entropy analysis in a cilia transport of nanofluid under the influence of magnetic field *Nucl. Eng. Technol.* **49** 1680–8

[38] Adesanya S O and Fakoya M B 2017 Second law analysis for couple stress fluid flow through a porous medium with constant heat flux *Entropy* **19** 498–509

[39] Bondareva N S, Sheremet M A, Öztop F H and Abu-Hamdeh N 2017 Entropy generation due to natural convection of a nanofluid in a partially open triangular cavity *Adv. Powder Technol.* **28** 244–55

[40] Astanina M S, Sheremet M A, Öztop F H and Abu-Hamdeh N 2018 MHD natural convection and entropy generation of ferrofluid in an open trapezoidal cavity partially filled with a porous medium *J. Mech. Sci.* **136** 493–502

[41] Nield D and Bejan A 2006 *Convection in Porous Media* 3rd edn (New York: Springer)

[42] Das K, Choi U, Yu W and Pradep T 2007 *Nanofluid Science and Technology* (New York: Wiley)

[43] Nield D and Kuznetsov A 2011 The Cheng–Minkowycz problem for natural convection about a vertical plate embedded in a tridisperse porous medium *Int. J. Heat Mass Transfer* **54** 3485–93

[44] Hamilton R L and Crosser O K 1962 Thermal conductivity of heterogeneous two-component system *Ind. Eng. Chem. Fundam.* **1** 187–91

[45] Timofeeva E V, Routbort J L and Singh D 2009 Particle shape effects on thermophysical properties of alumina nanofluids *J. Appl. Phys.* **106** 014304

[46] Akbar N S, Butt A W and Noor N F M 2014 Heat transfer analysis on transport of copper nanofluids due to metachronal waves of cilia *Curr. Nanosci.* **10** 807–15